Acta Cryst. (1996). B52, 616–627

Sodalite, $Na_4Si_3Al_3O_{12}Cl$: Structure and Ionic Mobility at High Temperatures by Neutron Diffraction

R. K. McMullan,[a] Subrata Ghose,[b]* Nobuhiko Haga[b,c] and Verner Schomaker[d]

[a]*Chemistry Department, Brookhaven National Laboratory, Upton, NY 11973, USA,* [b]*Mineral Physics Group, Department of Geological Sciences, University of Washington, Seattle, WA 98195, USA,* [c]*Faculty of Science, Himeji Institute of Technology, Harima Science Park, Kamigori, Ako, Hyogo 678-12, Japan, and* [d]*Department of Chemistry, University of Washington, Seattle, WA 98195, USA*

(*Received 22 June 1995; accepted 25 March 1996*)

Abstract

Crystal data: $Na_4Si_3Al_3O_{12}Cl$, cubic, space group $P\bar{4}3n$, $Z = 2$, $F(000) = 233.06$ fm, $\mu_n = 0.06\,cm^{-1}$, lattice parameter a_o (Å) [T] (K) at eight temperatures: 8.882 (1) [295]; 8.902 (2) [500]; 8.912 (1) [600]; 8.923 (1) [700]; 8.951 (2) [800]; 8.971 (1) [900]; 8.988 (1) [1000]; 9.037 (1) [1200]. The crystal structure has been determined at six temperatures ($295 \le T \le 1200$ K) based on neutron diffraction data with $(\sin\theta/\lambda) < 0.80$ Å^{-1}. Besides conventional parameters, the least-squares refinement model included thermal tensor parameters up to fourth-order for sodium and chlorine ($295 \le T \le 1200$ K) and up to third-order for oxygen ($T \ge 700$ K), together with the 1:1 coupled site occupancy factors of sodium and chlorine ($T = 1200$ K). The indices-of-fit, $wR(F^2)$, are in the range 0.015–0.028 with observation-to-parameter ratios from 7.0 to 8.6. Bond lengths and angles in the aluminosilicate framework have average e.s.d.'s less than 0.002 Å and 0.08°. Between 295 and 1200 K, the observed Si—O (Al—O) bond lengths differ by −0.015 Å (−0.012 Å); corrections for librating rigid SiO_4 (AlO_4) groups change the difference to +0.004 Å (+0.006 Å), compared with the 295 K value of 1.620 Å (1.741 Å). The unique Si—O—Al angle increases from 138.24° (295 K) to 146.87° (1200 K), while the Si and Al valence angles are virtually unchanged. Between 295 and 1200 K the [Na_4Cl] clusters expand with increases in the Na—Cl bond lengths of 0.200 Å, with simultaneous increases in Na—O bond lengths of 0.145 Å and decreases in the shortest Na···O contact distances of 0.126 Å. The thermal expansion of sodalite is attributed to the increasing amplitudes of coupled translational motion of the Na^+ ions and the librational motion of the [Al/SiO_4] tetrahedra, leading to the untwisting of the aluminosilicate framework. Maps of the probability density functions for Na^+ and Cl^- indicate ionic diffusion paths along ⟨111⟩ directions. There is a finite probability of finding the Na^+ ion within the plane of the next-nearest O atoms, suggesting that Na^+ jumps from an occupied to an unoccupied site in the next-nearest cage through the six-membered ring of [Al/SiO_4] tetrahedra.

1. Introduction

The structure of the mineral sodalite, $Na_8Cl_2Si_6Al_6O_{24}$, was determined by Pauling (1930) and refined by Löns & Schulz (1967) and Hassan & Grundy (1984) based on room-temperature X-ray diffraction data. Sodalite has the simplest tetrahedral aluminosilicate framework of a zeolite type, consisting of a space-filling arrangement of truncated octahedra defined by alternating Si and Al atoms at vertices and O atoms near the centers of connecting edges (Fig. 1). The chloride ions occur at centers of the truncated octahedra, surrounded by four sodium ions in a tetrahedral coordination. The sodium ions lie on threefold axes adjacent to six-membered rings of [SiO_4] and [AlO_4] tetrahedra and are fourfold coordinated to one chloride ion and three O atoms. Intersecting channels along ⟨111⟩ directions through the six-membered rings confer zeolitic properties on sodalite. The Na^+ ions in basic sodalite, $Na_8(OH)_2Si_6Al_6O_{24}$, can be completely and reversibly exchanged by Li^+, K^+ and Ag^+ ions at relatively low temperatures of ~360 K (Barrer & Falconer, 1956). For the mineral sodalite, electrical conductivity measurements on the blue and white forms show a marked increase in ionic conductivity above ~700 K (Annersten & Hassib, 1979) and a further abrupt increase above

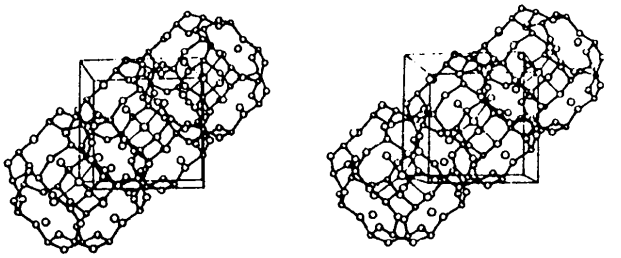

Fig. 1. Stereoview of the sodalite structure showing the truncated octahedra centered at (0,0,0), $(\frac{1}{2},\frac{1}{2},\frac{1}{2})$, (1,1,1) with the enclosed Na_4Cl groups.

~1100 K (Duba & Ghose, 1984). High ionic diffusion of Na^+ and Cl^- along the sodalite channels parallel to ⟨111⟩ is expected at high temperature, provided significant cation and anion vacancies exist. The thermal expansions of sodalite and structurally related compounds have been extensively studied by high-temperature powder X-ray diffraction (Taylor, 1968; Henderson & Taylor, 1978). These cubic structures are characterized by anomalous increases in their cell dimensions with temperatures over the range 293–1100 K.

In this paper we report single-crystal neutron diffraction refinements of sodalite at six temperatures in the range 295–1200 K. We discuss the thermal expansion in terms of the observed structural changes and ionic diffusion in terms of the anharmonicity of the Na^+ and Cl^- ions.

2. Experimental

The available sodalite crystals (Litchfield, Maine) were pale blue, irregular specimens, some of which exhibited faces of the form {110}. Electron microprobe analyses of ten fragments from this material gave average atom ratios: Na [3.98(5)], Si [3.06(3)], Al [2.97(3)], Cl [1.00(2)], where the e.s.d.'s in parentheses are derived from variations in the analyses. These elements and oxygen, reported as SiO_2 and Al_2O_3, accounted for 100.3(3)% of the total crystal composition. Potassium, magnesium, calcium, iron and sulfur were present in amounts less than 0.05%. Two crystals (Table 1) with good diffraction characteristics were selected for temperature-dependent measurements: sample S1 was used at 295–700 K and sample S2 at 800–1200 K. S1 was affixed to an aluminium pin with high-temperature cement; S2 was sealed in a vacuum inside a silica-glass capsule with silica-wool packing. Sample temperatures were controlled inside a vacuum furnace heated by a nichrome resistance element at $T \leq 700$ K and inside a furnace (Abrahams, Beuhler, Hamilton & Laplaca, 1973) heated by a Pt resistance element at $T > 700$ K.* The temperature stability was $\pm 1^\circ$ within the range 500–700 K and $\pm 5^\circ$ at 900 and 1200 K; larger and uncertain variations occurred at 800 and 1000 K due to malfunction of the furnace control element.

The diffraction data were measured at the Brookhaven High Flux Beam Reactor using monochromated neutron beams obtained by reflection from beryllium (002) planes. The three wavelengths used (Table 1) were calibrated against a KBr crystal ($a_0 = 6.6000$ Å). Intensity and cell dimension measurements were made first at 295, 500, 600 and 700 K, then at 900 and 1200 K. In addition, cell dimensions were obtained at 800 and 1000 K, prior to the 900 and 1200 K measurements. Heating at 1300 K caused crystal S2 to disintegrate abruptly after ~6 h, leaving fragments covered with a white powder assumed to be NaCl. The lattice parameters at each temperature were determined by least-squares fits of $\sin^2\theta$ values for 32 reflections in the range $47 < 2\theta < 54^\circ$. The intensity data were collected within three to six equivalent reciprocal lattice sectors [$|h|, |k|, |l| \leq 14$; $\sin\theta/\lambda \leq 0.79$ Å^{-1}] by the $\omega/2\theta$ step-scan method using scan-widths $\Delta 2\theta = 3.0^\circ$ for $\sin\theta/\lambda < 0.44$ Å^{-1}, $\Delta 2\theta = (K_1 + K_2 \tan\theta)^\circ$ for $\sin\theta/\lambda > 0.44$ Å^{-1}, where the dispersion constants K_1 and K_2, were determined for each crystal. Sectors were selected to avoid placing the furnace cables within the incident or diffracted beam paths. Counts were accumulated at each step for a preset count of the direct beam which required ~1.4 s. The intensities of two reflections monitored at ~3 h intervals for each data set were constant within ±2%. The integrated intensity I_{oi} for each reflection was obtained from the total scan counts by subtracting the background as estimated from the outer 10% parts of the scan. Variances, $\sigma_c^2(I_{oi})$, were derived from counting statistics. For reflections of sample S1, absorption corrections (de Meulenaer & Tompa, 1965; Templeton & Templeton, 1973) were applied using tabulated μ/ρ values (*International Tables for X-ray Crystallography*, 1962, Vol. 3). Transmission factors ranged between 0.984 and 0.986 or ~0.2%. No absorption corrections could be applied to the S2 data sets because the dimensions of the sample had not been obtained before it fragmented. Weak reflections affected by Al powder intensities from the vacuum furnace were deleted from the S1 data sets (295–700 K); no reflections were deleted from S2 sets (900 and 1200 K) since contributions from silica-glass scattering were negligibly small. Symmetry-equivalent F_o^2 ($I_o \sin 2\theta$) observations in each data set were averaged giving the independent reflections (Table 1) used in refinements. The variances $\sigma_o^2(F_o^2)$ taken for S1 data were averages of counting statistics values; those taken for S2 data were the larger of the population and counting statistics (Abrahams & Reddy, 1965).

3. Refinement

Initial values for coordinates were taken from the sodalite refinement by Löns & Schulz (1967). Refinements were carried out by the full-matrix least-squares program of Lundgren (1982). The residual $\Sigma w|F_o^2 - F_c^2|^2$ was minimized with weights $w = [\sigma_c^2(F_o^2) + (KF_o^2)^2]^{-1}$, where $K = 0.01$ and 0.00 for data sets of S1 and S2, respectively. Coherent neutron-scattering lengths (fm) for Na (3.63), Si

*Calibrations of the furnace control thermocouples were checked against the anorthite (Ghose, McMullan & Weber, 1993) $P\bar{1} \leftrightarrow I\bar{1}$ transition at 514 K (vacuum furnace) and the $\alpha \leftrightarrow \beta$ quartz transition at 846 K (Pt resistance furnace).

Table 1. *Crystal data and diffraction measurements for sodalite: $Na_4Si_3Al_3O_{12}Cl$*

Space group	$P\bar{4}3n$	
Z	2	
Crystal sample	1	2
Principal faces	{110}	{110}
Crystal shape	Irregular	Irregular
Weight (mg)	44.39	95.93
Volume* (mm^3) at 295 K	19.3	41.8
Maximum dimensions (mm)	2.6 × 2.9 × 3.5	5.5 × 5.2 × 4.5
Absorption coefficient μ_n (cm^{-1})	0.06	0.06
Wavelength† (Å)	1.0556 (1)	1.0505 (1)
		1.0495 (1)

	Temperature (K)					
Cell‡	295	500	600	700	900	1200
a_o (Å)	8.882 (1)	8.902 (2)	8.912 (1)	8.923 (1)	8.971 (1)	9.037 (1)
V (Å^3)	700.7 (2)	705.4 (5)	707.8 (2)	710.5 (2)	722.0 (2)	738.0 (5)
Density (g cm^{-3})	2.297	2.282	2.274	2.265	2.229	2.181
$\sin\theta/\lambda$ limit (Å^{-1})	0.79	0.79	0.79	0.79	0.79	0.79
Intensity data						
Equivalent sectors no. of reflections	4	4	4	6	3	3
Total§	926	946	988	1436	791	805
Independent	274	275	280	280	291	296
$R(F^2)_{int}$¶	0.019	0.028	0.036	0.029	0.021	0.028

*Computed from weight and density. †Wavelength λ: 1.0556 (295, 500, 600, 700 K); 1.0505 (800,1000 K); 1.0495 Å (900,1200 K). ‡ Lattice constant, a_o, measured at 800 [8.951 (2) Å], 1000 [8.988 (1) Å] and 1300 K [9.078 (2) Å]. § Excluding intensity monitor reflections and space extinctions (*hhl G*; $l = 2n + 1$). ¶ $\sum|F_{io}^2 - \bar{F}_o^2|/\sum\bar{F}_o^2$.

(4.149), Al (3.449), O (5.803) and Cl (9.579) were taken from the tabulation of Koester (1977). The variable parameters in each refinement included the free coordinates and U_{ij} thermal parameters, one scale factor and the isotropic secondary extinction parameter for type 1 crystals (Becker & Coppens, 1974). The data were marginally affected by extinction: Corrections ($\times F_o^2$) greater than 1.05 were applied to two reflections of the larger crystal S2. Varying the scattering lengths at Al and Si sites gave no significant improvements in fit indices nor produced changes $> 1.0\sigma$ in b_{Al} or $> 2.0\sigma$ in b_{Si}. The scattering lengths of Si and Al were reset to the above values in later refinement cycles. Difference-Fourier syntheses based on the harmonic refinements model showed similar features in residual density (Figs. 2*a–d*), increasing with temperature up to 4.0% of ρ_o maximum in the Fourier map at 1200 K. The largest density residuals occurred near sodium and chlorine sites at all temperatures, with those near oxygen sites increasing significantly at 700, 900 and 1200 K. Additional refinements were carried out to determine whether the residual density features could be described by anharmonic thermal vibrations. Anharmonic coefficients were introduced as variable parameters in the Gram–Charlier series expansion of the probability density functions (Johnson & Levy, 1974), using third- and fourth-order terms C_{ijk} and D_{ijkl} for sodium and chlorine, and C_{ijk} terms for oxygen. The crystal site symmetries of chlorine (T) and sodium (C_3) restrict the number of variable C_{ijk} and D_{ijkl} coefficients to 13 for the nonframework atoms. No symmetry constraints exist among the ten C_{ijk} oxygen coefficients. Each refinement converged readily, with last-cycle parameter shifts $< 0.01\sigma$. The strongest correlations occurred in the 1200 K refinement between sodium parameters: U_{11} and D_{1111} at 0.944; D_{1122} and D_{1123} at 0.933. The improvements in fits were highly significant (0.1% levels) in the R-factor ratio tests (Hamilton, 1965) when C_{ijk} and D_{ijkl} parameters of sodium and chlorine were included for all data sets and when C_{ijk} parameters of oxygen were included for data sets at 700–1200 K. To test for the possible loss of NaCl prior to crystal disintegration at 1300 K, the occupancy factors of sodium and chlorine were included as variables in refinements based on the 900 and 1200 K data. The refinements with independent occupancy factors failed to converge; 1:1 coupling with the sodium occupancy as the free parameter produced convergence with slightly improved fit only for the 1200 K data, giving a NaCl deficiency of 2.7 (4)%. Table 2 compares the indices-of-fit from the harmonic and anharmonic refinements at convergence. The final nuclear parameters* given in Table 3 are taken from refinements corresponding to the last entries of columns in Table 2. In the final ΔF maps the average

*Lists of structure factors and anharmonic coefficients have been deposited with the IUCr (Reference: CR0505). Copies may be obtained through The Managing Editor, International Union of Crystallography, 5 Abbey Square, Chester CH1 2HU, England.

Table 2. *Refinement conditions: free positional and harmonic thermal parameters U_{ij} varied for all atoms; third- and fourth-tensor coefficients, C_{ijk} and D_{ijkl} varied or fixed as indicated by refinement numbers 1–4; indices-of-fit $wR(F^2)$* and S† are given on first and second lines, respectively, for each refinement*

	Temperature (K)					
	295	500	600	700	900	1200
$N=$	265	265	268	267	291	296
(1) $V=19$	0.024	0.032	0.033	0.034	0.033	0.049
	1.185	1.417	1.420	1.480	2.131	1.761
(2) $V=31$	0.022	0.028	0.027	0.025	0.019	0.029
	1.110	1.249	1.173	1.098	1.233	1.644
(3) $V=41$				0.023	0.015	0.017
				1.037	1.012	0.990
(4) $V=42$						0.016
						0.928
Final						
Scale	0.1038(2)	0.1056(3)	0.1059(3)	0.1065(3)	0.0777(2)	0.0791(2)
g‡	0.57(8)	0.70(11)	0.60(10)	0.59(10)	1.00(8)	0.85(10)

(1) Harmonic U_{ij} refinements. (2) Anharmonic refinement; C_{ijk}, D_{ijkl} for Na and Cl. (3) Anharmonic refinement; C_{ijk}, D_{ijkl} for Na and Cl, C_{ijk} for O. (4) Anharmonic refinement; C_{ijk} for Na and Cl, C_{ijk} for O, site occupancy factor of Na. * $wR(F^2)=\sum w|F_o^2-F_c^2|^2/\sum(wF_o^2)^2]^{1/2}$. † $S=[\sum w|F_o^2-F_c^2|^2/(N-V)]^{1/2}$. ‡ Isotropic extinction factor $\times 10^3$ rad^{-1}.

$|\Delta\rho|_{max}$ is 1.1% of the Si peak in the ρ_o maps; the largest residual error (Fig. 2*h*), 2.2% of ρ_o(Si), occurs at the origin and may be attributed to the difference between least-squares and Fourier scaling.

4. Structural parameters

The atomic sites in Table 3 are fully and uniquely occupied within estimated errors of the analyses, except for the eightfold sodium and twofold chlorine sites at 1200 K. The loss of ~3% NaCl at 1200 K provides evidence for the accumulative effect of ion diffusion. Presumably, the temperature-enhanced diffusion rates of Na^+ and Cl^- result in the eventual crystal disintegration at 1300 K. Table (4*a*) lists the unique bond lengths and angles and short interaction distances, computed from the mean nuclear positions. The Si—O and Al—O bond lengths are subject to large thermal motion effects, particularly at the higher temperatures, as discussed later. Table 4(*b*) gives the slopes and

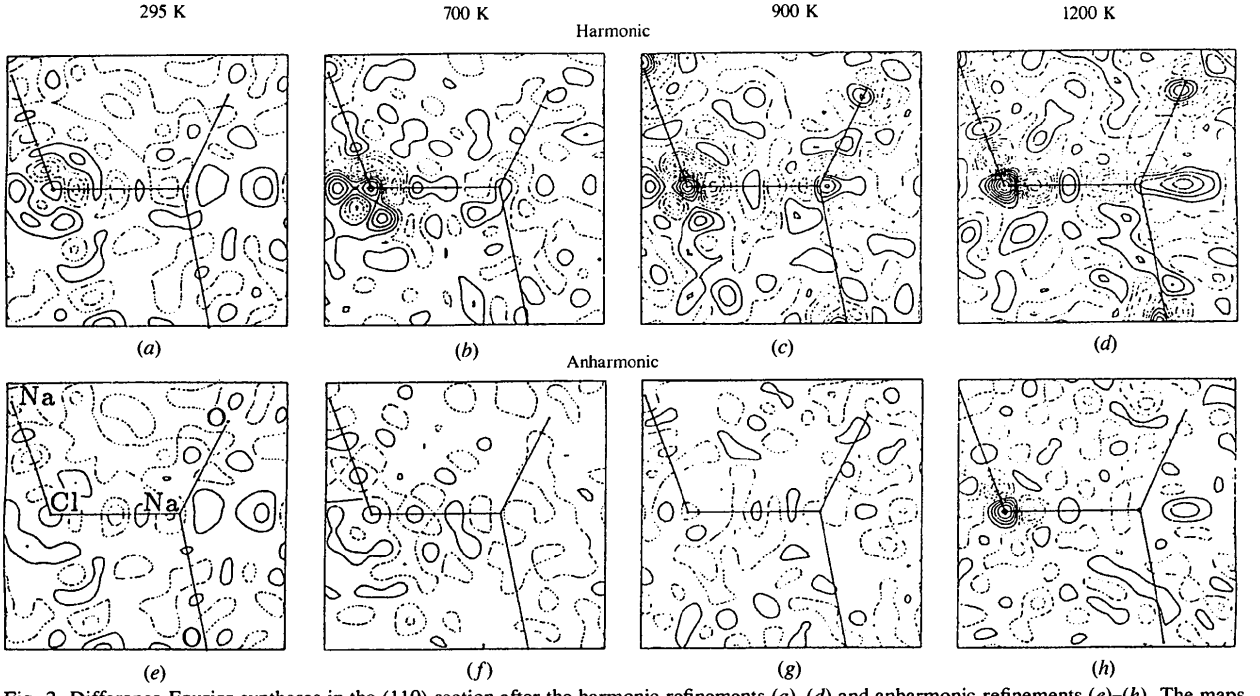

Fig. 2. Difference-Fourier syntheses in the (110) section after the harmonic refinements (*a*)–(*d*) and anharmonic refinements (*e*)–(*h*). The maps cover 6 × 6 Å and are oriented with (111) horizontal. Atom labels in (*e*) show the in-plane Na, Cl positions and the two O positions nearest the sections. The contour interval is 0.01 × 10^{-12} cm Å^{-3}, using dashed lines and solid lines for − and + values.

Table 3. *Atomic positions in sodalite: space group $P\bar{4}3n$*

Atom	Site	Symmetry	Coordinates		
O	24(*i*)	1	*x*	*y*	*z*
Na	8(*e*)	3	*x*	*x*	*x*
Si	6(*d*)	$\bar{4}$	$\frac{1}{4}$	0	$\frac{1}{2}$
Al	6(*c*)	$\bar{4}$	$\frac{1}{4}$	$\frac{1}{2}$	0
Cl	2(*a*)	23	0	0	0

Positional parameters and site occupancy factors of sodium (chlorine) *occ*(Na) = *occ*(Cl) fixed at 1.0 for $T < 1200$ K

	Temperature (K)					
	295	500	600	700	900	1200
x(O)	0.13925 (4)	0.13977 (6)	0.14005 (6)	0.1401 (1)	0.1409 (1)	0.1424 (1)
y(O)	0.43851 (4)	0.44075 (5)	0.44181 (5)	0.44347 (9)	0.4490 (1)	0.4582 (1)
z(O)	0.14954 (4)	0.15005 (6)	0.15030 (6)	0.1505 (1)	0.1513 (1)	0.1525 (1)
x(Na)	0.1778 (2)	0.1781 (2)	0.1782 (3)	0.1787 (2)	0.1818 (3)	0.1876 (5)
occ(Na)						0.973 (4)

Thermal parameters, $U_{ij} \times 10^4$ Å^2. The form of the temperature factor is: $T = T_2[1 + T_3 + T_4]$, where $T_2 = \exp(-2\pi^2 \sum_i \sum_j h_i h_j a_i^* a_j^* U_{ij})$; $T_3 = -(4\pi^3 i/3) \sum_i \sum_j \sum_k h_i h_j h_k C_{ijk}$; $T_4 = (2\pi^4/3) \sum_i \sum_j \sum_k \sum_l h_i h_j h_k h_l D_{ijkl}$, with T_3 and $T_4 = 0$ for silicon and aluminum; $T_4 = 0$ for oxygen at $T < 700$ K.

	Temperature (K)					
	295	500	600	700	900	1200
U_{11}(O)	111 (2)	172 (3)	200 (4)	228 (3)	334 (5)	430 (6)
U_{22}(O)	111 (2)	168 (2)	197 (2)	229 (2)	355 (2)	556 (4)
U_{33}(O)	111 (2)	168 (3)	193 (4)	225 (3)	323 (3)	449 (6)
U_{12}(O)	9 (2)	12 (3)	14 (3)	16 (3)	23 (4)	35 (4)
U_{13}(O)	50 (1)	81 (2)	94 (2)	112 (2)	167 (2)	230 (2)
U_{23}(O)	0 (2)	4 (3)	6 (3)	4 (3)	7 (4)	18 (4)
U_{11}(Na)	208 (6)	341 (10)	407 (10)	462 (9)	793 (18)	1266 (40)
U_{12}(Na)	12 (8)	2 (11)	16 (12)	30 (12)	101 (24)	470 (45)
U_{11}(Si)	59 (4)	81 (6)	96 (6)	110 (5)	139 (7)	207 (8)
U_{22}(Si) = U_{33}	68 (3)	98 (4)	109 (4)	126 (3)	193 (5)	248 (5)
U_{11}(Al)	67 (5)	92 (7)	101 (7)	118 (6)	171 (9)	201 (10)
U_{22}(Al) = U_{33}	70 (3)	100 (4)	119 (4)	136 (4)	192 (6)	248 (6)
U_{11}(Cl)	257 (5)	405 (7)	479 (7)	690 (5)	1247 (16)	1963 (17)

correlation coefficients for linear regressions of the distance and angle parameters on the unit-cell parameter over the range 295–1200 K. All parameters are fitted within 3 e.s.d.'s, except the Na—Cl distance (10 e.s.d.'s) and the angles O—Na—O (17 e.s.d.'s) and O—Na—Cl (5 e.s.d.'s).

The unit-cell dimensions in the range 295–1200 K (Table 1) are plotted against temperature in Fig. 3(*a*). The 295 (K) value [8.882 (1) Å] is in excellent agreement with room-temperature X-ray values [8.882 (1) Å (Hassan & Grundy, 1984) and 8.881 (1) Å (Henderson & Taylor, 1978)]. The cell expansion is represented by the least-squares fit $a_o = 8.868 + 1.3721 \times 10^{-5}T + 1.0656 \times 10^{-7}T^2$, within 2 e.s.d.'s.* The thermal expansion coefficient $\alpha[(da/dT)(1/a)]$, evaluated from the above polynomial, varies between $8.624 \times 10^{-6}K^{-1}$ at 295 K and $2.982 \times 10^{-5}K^{-1}$ at 1200 K. The cell parameters extrapolated to $T = 0$, 8.868 Å, agrees well with the value 8.866 Å obtained by a corresponding fit of the precise X-ray powder data (Henderson & Taylor, 1978) over the temperature range 293–1078 K. Above 700 K the X-ray and neutron data sets show significant differences corresponding to 0.0103 Å in a_o or 40 in T in extreme values. The discrepancy, whether in a_o or T, lies outside the expected error of measurement.

5. Discussion

5.1. *Thermal expansion*

The mechanism for thermal expansion of sodalite is implicit in Pauling's (1930) description of the structure (Fig. 1). With an increase in temperature the [SiO_4] and [AlO_4] tetrahedra (Figs. 4 and 5) rotate almost undistorted about their $\bar{4}$ axes parallel to *c* (*a* or *b*) with bending of the Si—O—Al linkages, by φ_{Al}–φ_{Si}, so as to progressively increase the shortest $Na^+ \cdots O$ mean distances and lattice constant. Changes in the shortest

* The exapansion data may be fitted with greater precision by two polynominals to account for the apparent discontinuity between 700 and 800 K, consistent with an anomalous increase in electrical conductivity observed above 700 K (Annersten & Hassib, 1979). The higher branch of the a_o *versus* T plot represents data obtained after crystal S2 (Table 1) had experienced prolonged heating at ~1000 K. The position and magnitude of the break may be dependent on the thermal history and/or methods of sample containment, but this remains uncertain.

Table 4(*a*). *Selected distances (Å) and angles (°), uncorrected for effects of thermal motion*

	Temperature (K)					
	295	500	600	700	900	1200
Si—O	1.6199 (4)	1.6181 (5)	1.6175 (5)	1.614 (1)	1.610 (1)	1.605 (1)
O···O*	2.7041 (8)	2.703 (1)	2.703 (1)	2.696 (2)	2.689 (2)	2.682 (2)
O···O†	2.6155 (6)	2.611 (1)	2.610 (1)	2.606 (2)	2.598 (2)	2.589 (2)
Al—O	1.7407 (4)	1.7393 (5)	1.7387 (5)	1.737 (1)	1.735 (1)	1.729 (1)
O···O*	2.8722 (8)	2.872 (1)	2.873 (1)	2.868 (2)	2.865 (3)	2.858 (3)
O···O†	2.8276 (6)	2.824 (1)	2.823 (1)	2.821 (2)	2.817 (2)	2.805 (2)
Na—O	2.3540 (4)	2.3762 (8)	2.3866 (7)	2.401 (1)	2.440 (1)	2.499 (2)
Na—O	3.084 (1)	3.071 (2)	3.066 (2)	3.057 (2)	3.022 (2)	2.958 (4)
Na—Cl	2.736 (1)	2.746 (1)	2.751 (1)	2.762 (1)	2.824 (2)	2.936 (3)
O—Al—O	111.18 (3)	111.31 (4)	111.40 (4)	111.28 (7)	111.32 (6)	111.51 (7)
O—Al—O	108.62 (1)	108.56 (2)	108.52 (2)	108.58 (3)	108.55 (3)	108.46 (3)
O—Si—O	113.15 (3)	113.28 (4)	113.36 (4)	113.24 (7)	113.28 (8)	113.37 (8)
O—Si—O	107.66 (1)	107.60 (2)	107.56 (2)	107.62 (4)	107.60 (4)	107.56 (4)
Al—O—Si	138.24 (2)	139.23 (3)	139.68 (3)	140.49 (6)	142.96 (6)	146.87 (7)
O—Na—O	103.46 (1)	103.27 (2)	103.18 (2)	103.25 (3)	103.93 (3)	105.28 (4)
O—Na—Cl	114.97 (4)	115.13 (6)	115.20 (6)	115.14 (7)	114.57 (8)	113.40 (13)

Table 4(*b*). *Regression lines for structure parameters $P_i(T)$ on $a_o(T)$ in the range 295 ≤ T ≤ 1200 K*

The slopes, $\text{Å}(P_i).\text{Å}^{-1}(a_o)$; $\text{deg}(P_i).\text{Å}^{-1}(a_o)$, and correlation coefficients are given on the first and second lines, respectively, for each parameter.

Si—O	O···O*	O···O†	Al—O	O···O*	O···O†	Na—O	Na—O	Na—Cl
−0.1004	−0.1509	−0.1782	−0.0734	−0.0822	−0.1460	0.9694	−0.7464	1.1455
−0.98813	−0.96007	−0.99441	−0.99485	−0.87636	−0.99361	0.99690	−0.99476	0.96042

O—Al—O	O—Al—O	O—Si—O	O—Si—O	Al—O—Si	O—Na—O	O—Na—Cl
1.83	−1.00	1.52	−0.80	54.70	8.29	−7.40
0.74965	−0.83446	0.61298	−0.66863	0.99878	0.74572	−0.75734

*O atoms related by $\bar{4}^2$. †O atoms related by $\bar{4}$.

$Na^+\cdots O$ contact distances with temperature appear to depend mainly on three motional effects: (1) increase in effective sizes of the $[Na_4Cl]$ clusters and O atoms with increasing harmonic thermal vibrations; (2) displacement of mean Na^+ positions along ⟨111⟩ from the fixed Cl^- positions with increasing anharmonic vibrations; (3) increased librational motion of the $[SiO_4]$ and $[AlO_4]$ groups. The increasing amplitudes of coupled translational motion of the Na^+ ion and the librational motion of the $[Al/SiO_4]$ groups lead to the untwisting of the aluminosilicate framework and account for the thermal expansion.

The static framework model of Hassan & Grundy (1984) provides a basis for estimating the effect of $[SiO_4]$ and $[AlO_4]$ group libration on the rotation and linkage angles, φ_{Si}, φ_{Al} and Si—O—Al, as shown in Fig. 4. From equations (5) and (6) of their paper, these angles can be evaluated using the unit-cell edge and assumed lengths for the Si—O and Al—O bonds, and O···O tetrahedral edges, E_{Si} and E_{Al}. To determine the effects of librational motion, φ_{Si} and φ_{Al}, Si—O—Al parameters evaluated from 295 K lengths were compared with those evaluated from foreshortened lengths (Table 4*a*) at higher temperatures. Differences between corresponding rotation and linkage angles increase significantly with temperature. At 1200 K the angles derived from variable lengths are 4.5° larger in φ_{Si} and φ_{Al} and 5.8° smaller in Si—O—Al than those at 295 K. Thus, the effect of bond foreshortening due to librational motion led to an apparent lessening of untwisting of the six-membered rings of tetrahedra.

5.2. *Temperature dependence of bond distances and angles*

The effect of thermal motion on Si—O and Al—O bond lengths was estimated from the U_{ij} parameters (Table 3) on the rough assumption that the $[SiO_4]$ and $[AlO_4]$ groups execute independent rigid-body motion. The analyses were based on the rigid-body model of Schomaker & Trueblood (1968) and were carried out with the program *THMA*13 of Trueblood (1978). By virtue of the site symmetry S_4, the rigid-body motion of each group is represented by six independent coefficients, two each for the translation, libration and screw tensors. Both groups show remarkable bond rigidity (Hirshfeld, 1976) over the entire range from 295 to 1200 K: the largest differences in mean-square displacements (m.s.d.'s), $\Delta_{Si,O}$ and $\Delta_{Al,O}$, along bond directions are 0.0009 (4) Å^2 for Si—O and 0.0011 (5) Å^2 for Al—O (Table 5*a*). In each group the differences $\Delta_{O,O}$ along two equivalent edges are 0.0 by virtue of the

twofold symmetry. However, four equivalent edges of each group appear to be particularly 'soft' or compressible, with differences $\Delta_{O,O}$ ranging from 0.0023 (3) to 0.0121 (7) Å^2 in [SiO_4] and from 0.0038 (3) to 0.0145 (7) Å^2 in [AlO_4] between 295 and 1200 K. The agreement indices, $wR(U_{ij})$, from the rigid-body least-squares fits (Table 5*b*) range from 0.053 to 0.107, with the fits for [SiO_4] being uniformly better than those for [AlO_4] over the entire temperature range. The librational amplitudes for each group, parallel and transverse to the symmetry axis, are listed in Table 5(*b*) and are shown as functions of temperature in Fig. 6. The Si—O

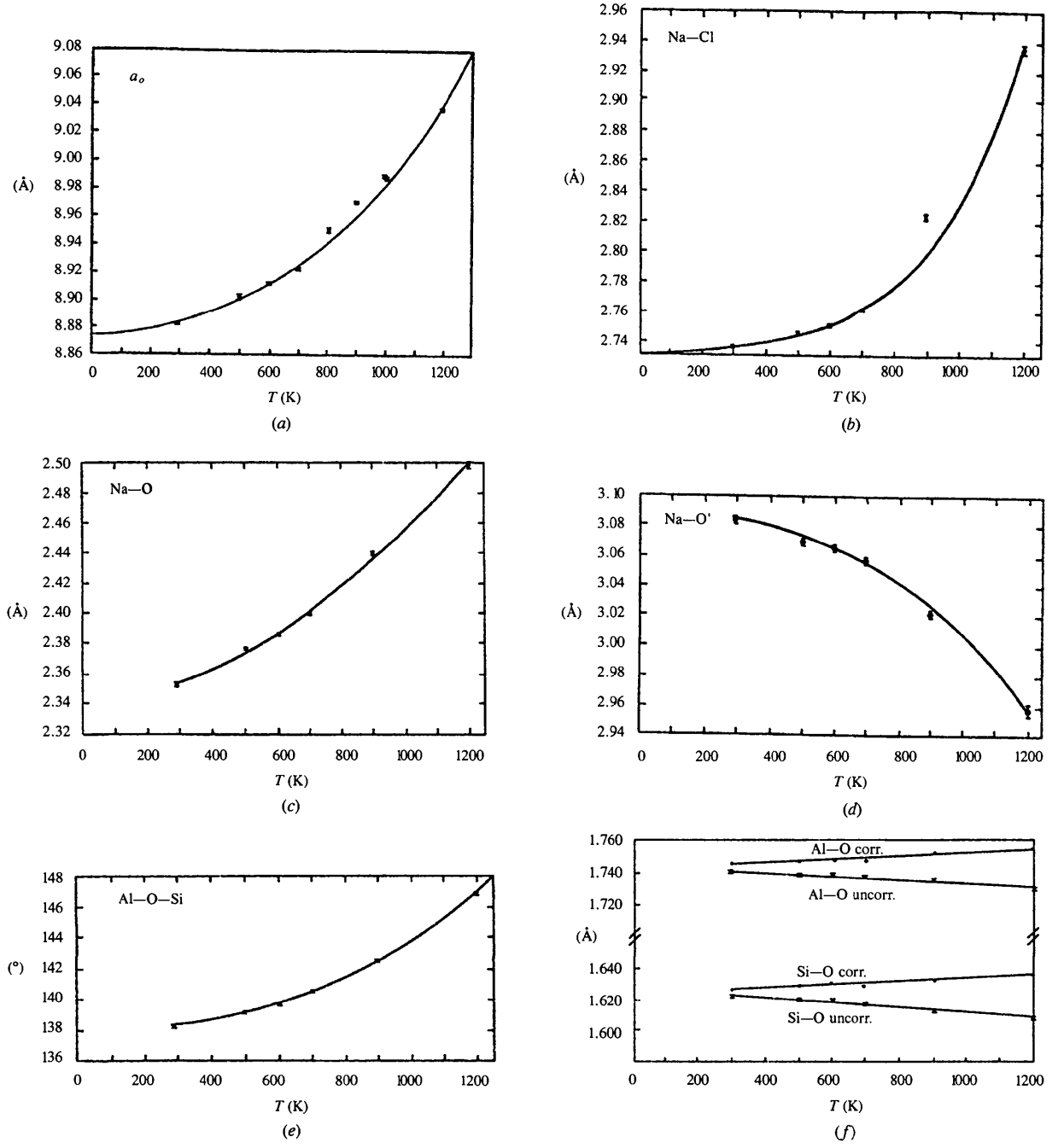

Fig. 3. Temperature dependence of (*a*) the lattice parameter; (*b*) Na—Cl bond length; (*c*) Na—O bond length; (*d*) shortest Na···O′ nonbonding distance: (*e*) Al—O—Si angle; (*f*) Al—O and Si—O bond lengths uncorrected and corrected for [AlO_4] and [SiO_4] rigid-body librational motion. The solid lines are included as guides for the eye.

Table 5(*a*). *Relative m.s.d.'s ($Å^2 \times 10^4$) of nuclei A and B along interaction directions, computed from the U_{ij} values of Table 4*

$\Delta(A,B) = \langle U_A^2 \rangle - \langle U_B^2 \rangle$ are the m.s.d.'s along the A—B directions.

	Temperature (K)					
	295	500	600	700	900	1200
A—*B*						
Si—O	1 (3)	4 (4)	9 (4)	4 (4)	4 (5)	4 (5)
O—O*	23 (3)	40 (4)	47 (4)	53 (4)	78 (7)	121 (7)
O—O†	0	0	0	0	0	0
Al—O	2 (2)	3 (4)	2 (4)	2 (4)	0 (5)	11 (5)
O—O*	38 (3)	55 (4)	63 (4)	75 (4)	110 (6)	145 (7)
O—O†	0	0	0	0	0	0
Na—O	92 (2)	173 (4)	205 (4)	221 (4)	392 (7)	473 (14)
Na—Cl	−25 (6)	−60 (9)	−41 (9)	−68 (9)	−253 (23)	+243 (43)

*Four edges of the tetrahedron formed by atoms related by $\bar{4}$ symmetry. † Two edges of the tetrahedron formed by atoms related by twofold symetry.

Table 5(*b*). *Rigid-body fit indices, $wR(U_{ij})$* and S† and libration values, L (deg^2), for the SiO_4 and AlO_4 groups*

	Temperature (K)					
	295	500	600	700	900	1200
SiO_4						
wR	0.063	0.063	0.070	0.061	0.053	0.080
S	2.92	3.33	3.89	4.42	4.85	7.21
e.s.d.	0.0012	0.0019	0.0023	0.0025	0.0038	0.0060
$L(1) \perp \bar{4}$	10.2 (3)	15.9 (4)	16.9 (4)	21.3 (5)	34.4 (6)	46.0 (7)
$L(3) \parallel \bar{4}$	7.8 (3)	13.0 (4)	18.4 (4)	19.9 (4)	29.0 (5)	55.0 (7)
AlO_4						
wR	0.107	0.088	0.094	0.090	0.076	0.098
S	2.92	4.65	5.23	6.35	6.90	8.72
e.s.d.	0.0020	0.0027	0.0031	0.037	0.0056	0.0070
$L(1) \perp \bar{4}$	8.1 (3)	13.5 (4)	16.2 (4)	18.9 (4)	28.3 (5)	36.6 (6)
$L(3) \parallel \bar{4}$	6.5 (3)	10.4 (4)	11.3 (3)	13.8 (4)	26.0 (5)	50.4 (7)

* $wR(U_{ij}) = [\sum w|U_o U_c|^2 / \sum wU_o^2)]^{1/2}$. † $S = [\sum w|U_o - U_c|^2 / (N-V)]^{1/2}$, where $N = 8$, the number of independent U_{ij} observations, and $V = 6$, the number of independent rigid-body parameters.

and Al—O bond lengths, uncorrected and corrected for librational motion, are compared in Table 6 and plotted as functions of temperature in Fig. 3(*f*). Between 295 and 1200 K, the differences in uncorrected values, −0.015 (Si—O) and −0.012 Å (Al—O), are changed by applied corrections to +0.004 and +0.006 Å (~2 e.s.d.'s), which, if meaningful, may indicate bond-stretching at the highest temperatures.

Increasing temperature produces shifts in the mean sodium positions along ⟨111⟩ directions and an effective expansion of the $[Na_4Cl]$ clusters in the aluminosilicate framework (Fig. 1). Between 295 and 1200 K the Na—Cl bond length increases by 0.200 Å, while the Na···Na distance increases by 0.328 Å. The Na—Cl bond length is shown as a function of temperature in Fig. 3(*b*). The Na—Cl—Na angles are fixed at the

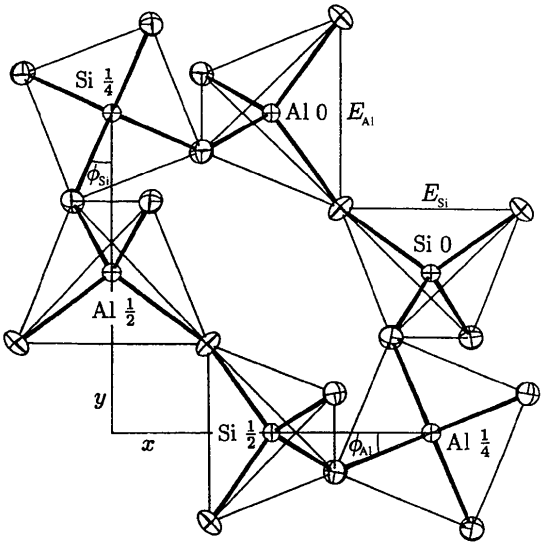

Fig. 4. Six-membered ring of vertex-linked $[AlO_4]$ and $[SiO_4]$ tetrahedra projected on the xy plane ($0 \le x, y \le \frac{1}{2}$), with z coordinates shown after atom labels. The edge lengths, E_{Al} and E_{Si}, and angles, φ_{Al} and φ_{Si}, are parameters of the geometric model for the sodalite framework (Hassan & Grundy, 1984), where the edges are between O atoms related by $\bar{4}^2$ symmetry and the angles are rotations parallel to z from the x $[AlO_4]$ and y $[SiO_4]$ axes. The thermal ellipsoids (295 K) are shown at 50% probability level (Johnson, 1976).

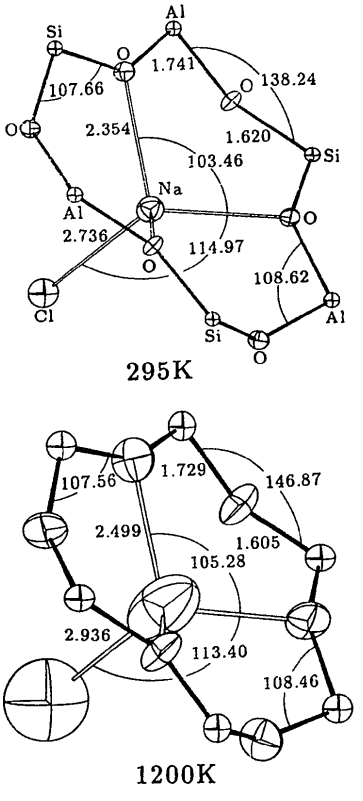

Fig. 5. The configuration of Na, Cl and $Al_3Si_3O_6$ atoms of the six-membered ring at 295 and 1200 K, with angles (°) and internuclear distances (Å) uncorrected for vibrational motion. Thermal ellipsoids are shown at 50% probability level, *cf.* Fig. 4.

Table 6. *Bond-length corrections for librational motion of SiO_4 and AlO_4*

	Temperature (K)					
	295	500	600	700	900	1200
Si—O	1.6199	1.6181	1.6175	1.614	1.610	1.605
	0.0046	0.0074	0.0084	0.010	0.016	0.024
	1.6245	1.6254	1.6261	1.624	1.626	1.629
Al—O	1.7407	1.7393	1.7387	1.737	1.735	1.729
	0.0040	0.0066	0.0077	0.009	0.014	0.022
	1.7447	1.7459	1.7464	1.746	1.749	1.751

tetrahedral value, 109.47°, by symmetry. In addition to chlorine, sodium is bonded to three of six O atoms of the six-membered rings (Fig. 5), in a trigonal pyramidal $[NaO_3Cl]$ coordination with C_3 symmetry. The Na—O bond length increases and the nonbonding Na···O′ distance decreases (Figs. 3*c* and *d*) as the $[Na_4Cl]$ cluster expands and the Si—O—Al angle widens (Fig. 3*e*) between 295 and 1200 K.

5.3. *Temperature-dependent displacement parameters*

The m.s.d.'s listed in Table 7(*a*) have been fitted to linear functions of temperature. The results are summarized in Table 7(*b*). Linearity is an assumed requirement for purely harmonic motion. Based on the criteria-of-fit, the m.s.d.'s of Al and Si from 295 to 1200 K can be described as harmonic with zero residual vibrations at 0 K within 3 e.s.d.'s. Oxygen $U1$(O), but not $U2$(O) or $U3$(O), is also linear with temperature within accepted limits. As seen in Fig. 5, the approximate directions of these displacements are: $U1$(O) parallel to the Al···Si vector, $U3$(O) along the bisector of the Al—O—Si angle and $U2$(O) normal to the Al—O—Si plane. Thus, while harmonic motion may be ascribed to oxygen in the Al—O and Si—O bond directions, the behavior of oxygen in Al—O—Si bending and wagging shows contributions from anharmonic vibrations or positional disorder. For sodium, the $U1$(Na) components transverse to the ⟨111⟩ direction (Fig. 5) conform remarkably well to requirements of harmonic motion; however, $U3$(Na) lying along ⟨111⟩ departs strongly from linearity, having a temperature dependence similar in form to that of the Na—Cl bond length shown in Fig. 3(*b*). The $U1$(Cl) components also show similar dependences, consistent with a strong mutual interaction between the m.s.d.'s of Na and Cl along the ⟨111⟩ direction of bonding. The residuals of $U3$(Na) and

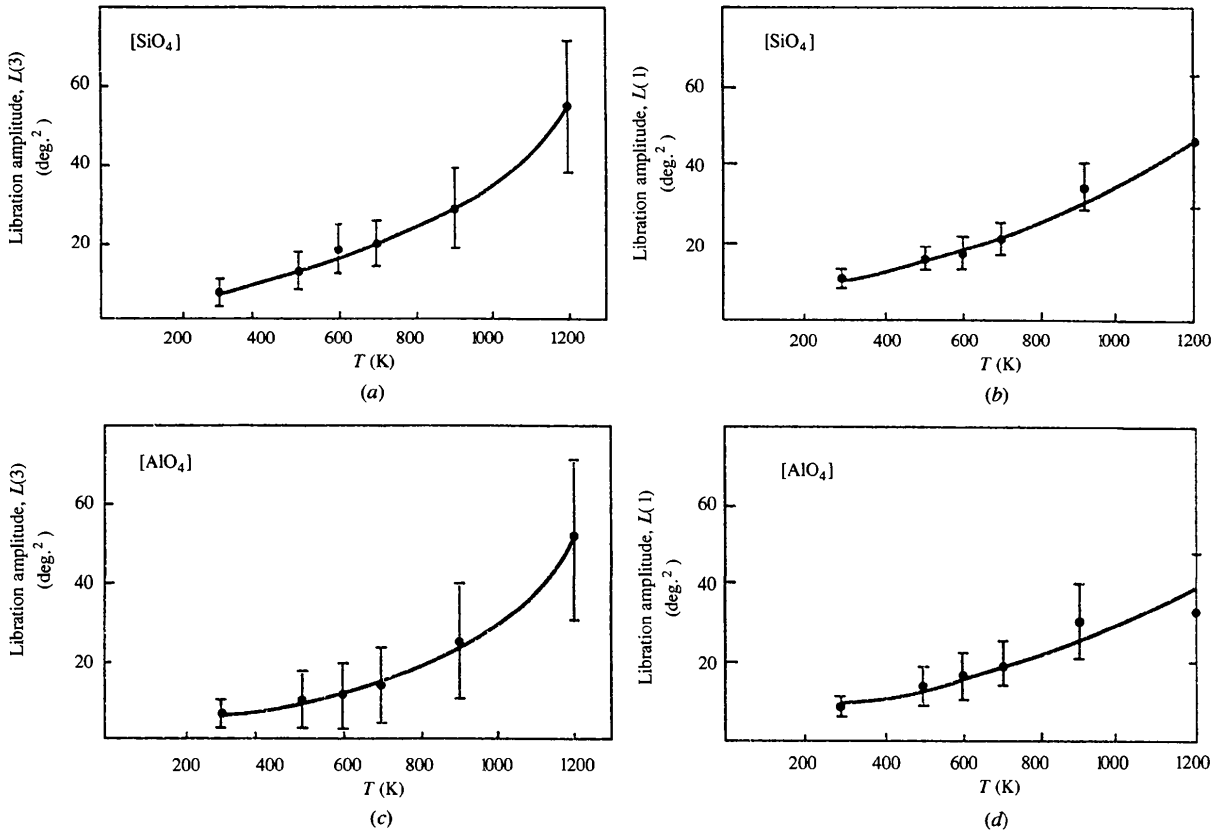

Fig. 6. Temperature dependence of the libration parameters for $[SiO_4]$: (*a*) $\|\bar{4}$, (*b*) $\perp \bar{4}$; and for $[AlO_4]$: (*c*) $\|\bar{4}$, (*d*) $\perp \bar{4}$.

Table 7(*a*). *Principal components of atomic m.s.d.'s (Å²) computed from U_{ij} parameters in Table 3*

	Temperature (K)					
	295	500	600	700	900	1200
*U*1(Al)	0.0067 (5)	0.0092 (7)	0.0101 (7)	0.0118 (6)	0.0171 (9)	0.0205 (11)
*U*3(Al)	0.0070 (3)	0.0100 (4)	0.0119 (4)	0.0136 (4)	0.0192 (6)	0.0252 (6)
*U*1(Si)	0.0059 (4)	0.0081 (5)	0.0096 (5)	0.0110 (5)	0.0139 (7)	0.0209 (9)
*U*3(Si)	0.0068 (2)	0.0098 (3)	0.0109 (4)	0.0126 (5)	0.0193 (4)	0.0251 (5)
*U*1(O)	0.0060 (1)	0.0088 (2)	0.0103 (2)	0.0114 (3)	0.0161 (2)	0.0213 (3)
*U*2(O)	0.0111 (1)	0.0167 (2)	0.0196 (2)	0.0228 (3)	0.0353 (3)	0.0549 (4)
*U*3(O)	0.0161 (2)	0.0252 (2)	0.0293 (3)	0.0340 (4)	0.0498 (4)	0.0687 (4)
*U*1(Na)	0.0195 (5)	0.0339 (7)	0.0391 (8)	0.0431 (1)	0.0692 (17)	0.0867 (39)
*U*3(Na)	0.0232 (6)	0.0345 (8)	0.0438 (9)	0.0522 (10)	0.0995 (20)	0.2267 (20)
*U*1(Cl)	0.0257 (5)	0.0405 (7)	0.0479 (7)	0.0590 (10)	0.1247 (16)	0.1963 (17)

Table 7(*b*). *Least-squares fits of m.s.d.'s (Table 7a) to lines $U = A + B \times T$*

	$A \times 10^3$	$B \times 10^5$	*wR**	⟨Δ⟩†	⟨Δ/σ⟩
*U*1(Al)	1.6 (7)	1.54 (11)	0.062	0.0007	0.9
*U*3(Al)	0.6 (4)	1.98 (6)	0.051	0.0007	1.5
*U*1(Si)	0.9 (6)	1.51 (9)	0.062	0.0007	1.1
*U*3(Si)	0.5 (3)	1.94 (5)	0.075	0.0010	3.2
*U*1(O)	1.0 (3)	1.63 (3)	0.045	0.0005	1.8
*U*2(O)	−1.7 (3)	3.97 (3)	0.135	0.0031	11.4
*U*3(O)	−2.6 (4)	5.59 (4)	0.061	0.0021	6.6
*U*1(Na)	−0.9 (9)	6.8 (2)	0.072	0.0034	2.2
*U*1(Na)	14.9 (11)	10.9 (2)	0.218	0.0257	16.1
*U*1(Cl)	23.3 (10)	13.4 (1)	0.276	0.0200	16.7

* As defined in Table 5(*b*). † ⟨Δ⟩ = average $|U(\text{obs}) - U(\text{calc})|$ Å².

*U*1(Cl), respectively, 0.0149 and 0.0233 Å², at 0 K indicate that these atomic displacements contain positional disorder which is not accounted for by time-averaged vibrations. It is suggested that Na and Cl lie in shallow potential wells and vibrate with large amplitudes sufficient for their redistribution between energy states at the measurement temperatures. Under this assumption, there is no clear distinction between static and dynamic disorder. However, useful information on atomic displacements in sodalite can be obtained by examining the temperature-dependent changes in the probability density functions derived from the observed U_{ij}, C_{ijk} and D_{ijkl} parameters.

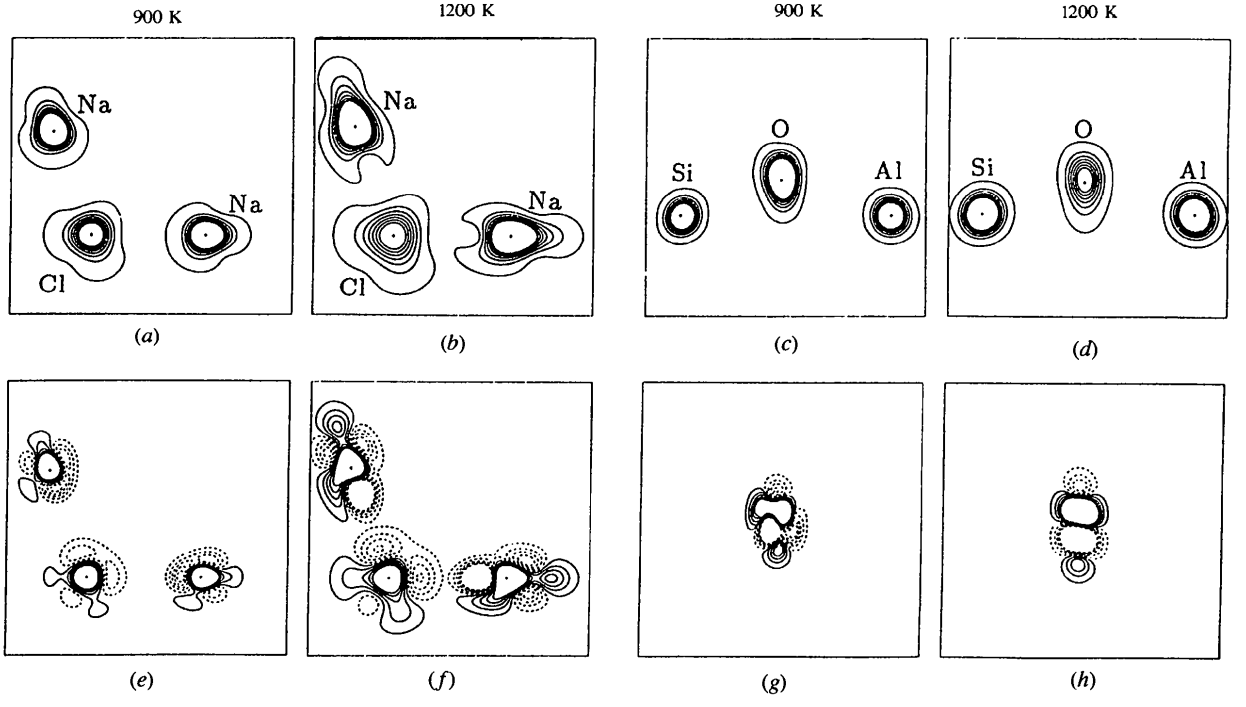

Fig. 7. Sections through the probability density functions at 900 and 1200 K for Na and Cl within the [110] plane and for Si, Al and O within the plane of the three atoms. The functions are evaluated from vibration tensors up to fourth order for Na and Cl, up to third order for O and of second order for Si and Al. The plots measure 7 × 7 Å for Na and Cl and 4 × 4 Å for Si, O and Al. Plots (*a*)–(*d*) show the total probability density functions with the highest and lowest contours enclosing 50 and 98% probability levels, respectively. (*e*)–(*h*) show contributions of the third- and fourth-order tensor components corresponding to plots (*a*)–(*d*).

5.4. *Effects of anharmonic displacements*

The anharmonic coefficients C_{ijk} and D_{ijkl} of Na and Cl become increasingly more significant with increasing temperature; the C_{ijk} coefficients of oxygen are significant only at 900 and 1200 K. The probability density functions at displacements **u** from nuclear positions have been mapped in two critical planes at 900 and 1200 K (Fig. 7) using a program of Craven & Weber (1985). The complete probability density functions (Figs. 7*a–d*), $\rho_2(\mathbf{u})[1 + \rho_3(\mathbf{u}) + \rho_4(\mathbf{u})]$, where $\rho_2(\mathbf{u})$ is the Gaussian probability density function derived from the U_{ij} parameters and $\rho_3(\mathbf{u})$ and $\rho_4(\mathbf{u})$ are the anharmonic components derived from the third- and fourth-order thermal tensor coefficients (Johnson & Levy, 1974), have no negative regions greater than the computed e.s.d.'s. Anharmonic parts of these probability density functions, $\rho_2(\mathbf{u})[\rho_3(\mathbf{u}) + \rho_4(\mathbf{u})]$, are mapped over the same planes in Figs. 7(*e*)–(*h*).

The anharmonic terms significantly modify the Gaussian probability density functions in the following ways. The plots for Cl^- at (000) with point symmetry T show positive tetrahedral lobes directed along the bisectors of the Na—Cl—Na bond angles and towards the next-nearest Na^+ ion at $(\bar{x}\bar{x}\bar{x})$ in the adjacent cages (Figs. 7*a* and *b*). The maps for Na^+ at (xxx) with point symmetry C_3 show approximate tetrahedral symmetry; one prominent positive lobe is directed along [111] towards the next nearest Cl^- ion and three equivalent positive lobes lie approximately along ⟨110⟩ directions. These features are more pronounced in Figs. 7(*e*) and (*f*), where the anharmonic contributions to the total probability density functions are represented. On these maps, negative regions lie along the nearest-neighbor Na^+–Cl^- and Na^+–O^{2-} directions, consistent with abruptly rising potential energy barriers at atomic contact.

5.5. *Ionic diffusion paths*

The probability density function maps indicate diffusion paths for Na^+ and Cl^- within the aluminosilicate framework along ⟨111⟩ channels defined by the six-membered rings. There is a finite probability of finding the Na^+ ion within the plane of the three next-nearest oxygen ions (Fig. 5), suggesting a significant probability of Na^+ jumping from an occupied (xxx) position to an unoccupied $(\bar{x}\bar{x}\bar{x})$ position in the next nearest cage through the six-membered ring. Simultaneous occupancy of all four $(\bar{x}\bar{x}\bar{x})$ positions by Na^+ ions will create an $[Na_4Cl]$ configuration which is enantiomorphous [related by $C_i(\bar{1})$] with the original configurations with Na^+ ions at (xxx) positions. One possible scenario to allow this foresees a Na^+ ion jumping from one cage to the next, where an Na^+ ion at an (xxx) position is vacant; the incoming Na^+ ion will occupy an $(\bar{x}\bar{x}\bar{x})$ position because of the lowest energy barrier that exists between the occupied (xxx) and the unoccupied nearest-neighbor $(\bar{x}\bar{x}\bar{x})$ positions. To achieve this configuration, the three Na^+ ions at the (xxx) positions must move in concert to the three vacant nearest neighbor $(\bar{x}\bar{x}\bar{x})$ positions. This rotational motion is indicated by the three equivalent lobes directed approximately along ⟨110⟩ in the probability density function plots for Na^+.

The jump of an Na^+ ion from the (xxx) position to the $(\bar{x}\bar{x}\bar{x})$ position though the six-membered ring requires a reverse puckering of the ring; this means a switching of the oxygen positions from (xxx) to $(\bar{x}\bar{x}\bar{x})$ positions separated by a distance of 0.75 Å. The double maxima in the skew symmetric plot of the C_{ijk} coefficients of the O^{2-} ion (Figs. 7*g* and *h*) likely indicate a response to this occurrence. These features might be precursors of a possible impending phase transition from an ordered [(xxx) position occupied in space group $P\bar{4}3n$] to a disordered centrosymmetric Na^+ configuration [(xxx) and $(\bar{x}\bar{x}\bar{x})$ positions occupied in space group $Pm3n$] with the Al/Si positions relatively unchanged. Discontinuities in the a_o *versus* T curve for Br^- and I^- sodalites at 1283 and 1083 K (Henderson & Taylor, 1978) may indicate such a phase transition.

The neutron data collection and a large part of the computations were carried out at Brookhaven National Laboratory under contract DE-AC02-76CH00016 with the US Department of Energy and supported by its Office of Basic Energy Sciences. This work was supported in part by NSF grants EAR 8719638 and EAR 9117389 (SG) . We wish to thank Professor V. S. Mallory, Burke Museum, University of Washington, for the sodalite sample and Dr Scott Kuehner, University of Washington, for the electron microprobe analyses. We are grateful to the late Joseph Henriques for technical assistance.

References

Abrahams, S. C. & Reddy, J. M. (1965). *J. Chem. Phys.* **43**, 2533–2543.

Abrahams, S. C., Beuhler, E., Hamilton, W. C. & Laplaca, S. J. (1973). *J. Phys. Chem. Solids,* **34**, 521–532.

Annersten, H. & Hassib, A. (1979). *Can. Miner.* **17**, 39–46.

Barrer, R. M. & Falconer, J. D. (1956). *Proc. R. Soc. Sect. A,* **236**, 227–249.

Becker, P. J. & Coppens, P. (1974). *Acta Cryst.* A**30**, 129–147.

Craven, B. M. & Weber, H.-P. (1985). *Computer Program NOOT for Least Squares Refinement with Neutron Diffraction Data.* Crystallography Department, University of Pittsburgh, USA.

Duba, A. G. & Ghose, S. (1984). Unpublished.
Ghose, S., McMullan, R. K. & Weber, H.-P. (1993). *Z. Kristallogr.* **204**, 215–237.
Hamilton, W. C. (1965). *Acta Cryst.* **18**, 502–510.
Hassan, I. & Grundy, H. D. (1984). *Acta Cryst.* B**40**, 6–13.
Henderson, C. M. B. & Taylor, D. (1978). *Phys. Chem. Miner.* **2**, 761–769.
Hirshfeld, F. L. (1976). *Acta Cryst.* A**32**, 239–244.
Johnson, C. K. (1976). *ORTEP*II. Report ORNL-5138. Oak Ridge National Laboratory, Tennessee, USA.
Johnson, C. K. & Levy, H. A. (1974). *International Tables for X-ray Crystallography*. Vol. IV, p. 316. Birmingham: Kynoch Press. (Present distributor Kluwer Academic Publishers, Dordrecht.)
Koester, L. (1977). *Springer Tracts in Modern Physics, Neutron Physics*, edited by G. Höhler, p. 36. Berlin: Springer.
Löns, J. & Schulz, H. (1967). *Acta Cryst.* **23**, 434–436.
Lundgren, J.-O. (1982). Report UUIC-B13-4-05. Institute of Chemistry, University of Uppsala, Uppsala, Sweden.
Meulenaer, J. de & Tompa, H. (1965). *Acta Cryst.* **19**, 1014–1018.
Pauling, L. (1930). *Z. Kristallor.* **74**, 213–225.
Schomaker, V. & Trueblood, K. N. (1968). *Acta Cryst.* B**24**, 63–76.
Taylor, D. (1968). *Miner. Mag. London,* **36**, 761–798.
Templeton, L. K. & Templeton, D. H. (1973). *Abstr. Am. Crystallogr. Assoc. Meet.* p. 143. Storrs, Connecticut, USA.
Trueblood, K. N. (1978). *Acta Cryst.* A**34**, 63–76.